Rare Met.
https://doi.org/10.1007/s12598-xxx-xxxxx-x

RARE METALS

ORIGINAL ARTICLE:

Enhanced near-room-temperature thermoelectric performance in GeTe

Xian Yi Tan, Jinfeng Dong*(iD 0000-0002-3026-8054), Ning Jia, Hongxia Zhang, Rong Ji, Ady Suwardi, Zhiliang Li, Qiang Zhu, Jianwei Xu, Qingyu Yan*(iD 0000-0003-0317-3225)

Received:*** / Revised: *** / Accepted: ***

Abstract GeTe is an excellent mid-temperature thermoelectric material with high *ZT* values at temperatures over 600 K. Its near-room-temperature performance is less studied due to the intrinsic high carrier concentration. Here, we successfully enhance the Seebeck coefficient of GeTe from ~30 μV/K to 220 μV/K at 300 K, which is achieved by $AgInSe_2$ alloying and Bi doping. It is demonstrated that Bi doping helps to optimize the Seebeck coefficient without deteriorating the intrinsic electrical transport properties of the matrix. A high room-temperature PF of ~ 11 $\mu Wcm^{-1}K^{-2}$ is achieved for a wide range of Bi doped samples. The simultaneously introduced abundant point defects cause mass and strain fluctuations, which decreased the lattice thermal conductivity (κ_L) to a low value of 0.6 $Wm^{-1}K^{-1}$ at 300 K. Thanks to the synergetic effects of Bi doping in $AgInSe_2$-alloyed GeTe, a high room-temperature *ZT* value of 0.46 is obtained together with a high *ZT* value of 1.1 at 523 K.

Keywords thermoelectric, GeTe, thermal conductivity, room-temperature *ZT*

Supplementary Information The online version contains supplementary material available at…

X.Y. Tan, J. Dong*, N. Jia, Q. Yan*
School of Materials Science and Engineering, Nanyang Technological University, 50 Nanyang Avenue, 639798, Singapore.
e-mail: jinfeng.dong@ntu.edu.sg, alexyan@ntu.edu.sg

X.Y. Tan, R. Ji, A. Suwardi, Q. Zhu, J. Xu
Institute of Materials Research and Engineering, Agency for Science, Technology and Research, 2 Fusionopolis Way, 138634, Singapore.

H. Zhang, Z. Li
Key Laboratory of High-Precision Computation and Application of Quantum Field Theory of Hebei Province, College of Physics Science and Technology, Hebei University, Baoding 071002, China

1 Introduction

Thermoelectric devices, which are capable of converting waste heat into electrical energy and enabling solid-state cooling in a green and quiet manner, has received soaring attention due to the rising concerns of global energy shortage and pollution to the ecosystem [1-3]. The efficiency of a thermoelectric module is related to the performance of its thermoelectric materials, which is characterized by the dimensionless figure of merit *ZT*. The *ZT* value can be determined by the Seebeck coefficient (*S*), electrical resistivity (ρ), thermal conductivity (κ) and absolute temperature (*T*) through the equation: $ZT = S^2\rho^{-1}\kappa^{-1}T$ [4-6]. While these physical parameters are closely related to each other, two other important parameters, namely the quality factor (*B*) and reduced Fermi level (η), can be applied to better understand and guide the development of thermoelectric materials through the equation $ZT=f(B, \eta)$ [7, 8].

As a hot research topic, the family of thermoelectric materials has expanded tremendously [9], where novel materials such as layered compound SnSe [10, 11] and $Sb_2Si_2Te_6$ [12], copper-based chalcogenide [13, 14], $Mg_3(Sb, Bi)_2$ [15, 16] and half Heusler alloys [17, 18] have emerged. Among them, GeTe has recently been demonstrated to be a promising medium-temperature thermoelectric material with an outstanding *ZT* >2 [19, 20]. Various attempts have been made to elucidate the underlying mechanisms and further enhance the thermoelectric performance of GeTe. Particularly, utilizing the rhombohedral-to-cubic phase transition, a subtle tuning of the structure can lead to an ideal band convergence of valence band maxima [21, 22]. In tackling the intrinsic excessive Ge vacancies, Ge self-compensation and Cu doping were found to lessen the impact of Ge vacancies on electronic mobility [23, 24]. Taking the advantage of the domain structure in GeTe, mesoscopic structure such as the charged domain wall or vacancy layers have been introduced to dramatically reduce

the thermal conductivity [25, 26]. Phase mapping also demonstrated that proper thermal treatment can result in the Spinodal fluctuation in Sb-doped GeTe, achieving a *ZT* value of >2.6 at 723 K [27]. Nano particle addition, entropy engineering and decreasing phase transition temperature have also proven to be effective method in tuning the properties of GeTe [28-32]. High-performance GeTe based module for power generation has also been reported [33].

Compared to the medium temperature thermoelectric properties of GeTe, near-room temperature thermoelectric properties are less studied. The main obstacle is the intrinsically high carrier concentration (~10^{21} cm^{-3}), which induces a very low Seebeck coefficient (<50 μV/K). Such a carrier concentration not only leads to low Seebeck coefficient that deviates largely from the optimal range (170-200 μV/K) for room temperature applications, but also results in an extremely high electronic thermal conductivity. The lattice thermal conductivity of pristine GeTe is also far from the satisfactory value and current studies of GeTe only realize a very low lattice thermal conductivity due to the more intensified scattering of phonons at high temperature, which further hinders the improvement of near-room-temperature *ZT*. The adjustable electronic properties of GeTe and the synthetic methods developed for decreasing the thermal conductivity have promised the possibility for enhancing its near-room-temperature *ZT* [31]. Also, Pb alloying has been proven to increase the room-temperature *ZT* significantly, demonstrating the potential of GeTe as a near room-temperature thermoelectric material [34, 35]. But the use of Pb is less favorable due to its toxicity.

In this work, $AgInSe_2$ was first alloyed into GeTe to decrease the lattice thermal conductivity, which was suppressed from >1.5 $Wm^{-1}K^{-1}$ to 0.75 $Wm^{-1}K^{-1}$ at 300K. The introduction of In also enhances the Seebeck coefficient to 70 μV/K due to its ability to induce a resonant level near the valance band edge [36]. Further Bi doping increases Seebeck coefficient to 180-220 μV/K at 300 K without causing noticeable deterioration to the intrinsic electrical transport properties. The lattice thermal conductivity decreases to a low value of ~0.6 W $m^{-1}K^{-1}$ at 300 K, which is induced by the scattering of phonons due to the various point defects. Based on the synergy of the above factors, the room-temperature *ZT* value was improved from 0.05 for pristine GeTe to 0.46 for AIS8-Bi8 sample as well as a high *ZT* of 1.1 at 523 K.

2 Experimental

Ge (pieces, 99.999%), Te (chunks, 99.99%), Ag (powder, 99.9%), In (powder, 99.9%), Se (lump, 99.99%) and Bi (lumps, 99.99%) were adopted as raw materials and were weighted according to the stoichiometric ratio ((1-*x*)GeTe-*x*$AgInSe_2$, labelled as AIS series). For Bi doping samples, the percentage of Bi is calculated according to the total cation number and labelled as AIS8-Bi series. They were then loaded into quartz ampules and flame-sealed under vacuum. Subsequently, the quartz ampules were placed into a box furnace and heated to 950 ˚C within 10 h. Before quenching into ice water, they were held at 950 ˚C for 6h. The quenched ampules were put back into the furnace for annealing at 550 ˚C for 72h. The synthesized samples were ground into fine powders with a mortar and pestle. The obtained powders were loaded into graphite dies and consolidated at 550 ˚C for 5 min under a pressure of 40 MPa (Ed-PasIVJ, 6T-3P-30, Japan). All the pellets have a high density of over 98 %.

The phase purity was examined using the ground powders by X-ray diffractometer (XRD) with Cu target (D8 Advance, Bruker, Germany). Freshly broken surfaces and finely polished surfaces of the pellet samples were used to identify the morphology and elemental distribution respectively, with a scanning electron microscope (SEM, JEOL JSM 7600F, Japan). Bar shaped and disc-like samples were cut to test the thermoelectric performance. The electrical resistivity and Seebeck coefficient were measured using an electrical resistivity/Seebeck coefficient measuring system (ZEM3, Ulvac-Riko, Japan). The thermal conductivity was calculated by the equation: $\kappa = DC_pd$, where D denotes thermal diffusivity and is obtained using the laser flash method (LFA 457, Netzsch, Germany), C_p is the specific heat capacity adopted by Dulong-Petit approximation, d represents density that was determined by Archimedes method.

3 Results and discussion

3.1 Influence of $AgInSe_2$ alloying on GeTe

We first investigated the effects of $AgInSe_2$ alloying on the phase structure and thermoelectric performance of GeTe. As shown in the XRD patten of powdered GeTe with various contents of AgInSe2 alloying (Fig. 1a**)**, all samples are well-indexed to α-GeTe, where the diffraction peaks shift slightly to higher 2θ values with increasing $AgInSe_2$ content. This is most likely due to the lattice contraction caused by the smaller Se^{2-} ions (ionic radius: 198 pm) replacing the larger Te^{2-} ions (ionic radius: 221 pm) in the GeTe lattice, which also overwhelms the lattice expansion from the larger ionic size of Ag^{+} (ionic radius: 115 pm) and In^{3+} (ionic radius: 80 pm) as compared to Ge^{2+} (ionic radius: 72 pm) [37]. The typical double peak of rhombohedral structure at 2θ = 43° approaches each other, indicating the rhombohedral structure is evolving towards cubic structure after $AgInSe_2$ alloying. After adding more than x=8% in (1-x)GeTe-$x$$AgInSe_2$, a minor secondary phase peak appeared, as indicated by the black arrow, which is related to In-Te phases. Ge

precipitates, which is common for GeTe, were observed in the SEM image and highlighted (Fig. 1b to Fig. 1d**)**. Besides Ge, no other secondary phases or elemental segregation have been observed.

All the $AgInSe_2$-alloyed GeTe samples display degenerate semiconductor behaviors, as indicated by the monotonically increased Seebeck coefficient and electrical resistivity with increasing temperature (Fig. 2a and Fig. 2b). With the increase of $AgInSe_2$ alloying content, the Seebeck coefficient gradually increases at temperatures below 600 K and reached ~70 μV/K at 300K for x=8% or 10% samples. This enhanced Seebeck coefficient, which is comparable to that of In-doped GeTe reported in other works, is most likely due to the resonant level near the valence band maximum induced by In [38, 39]. Meanwhile, due to the introduction of foreign atoms as well as the higher effective mass from In doping, the electrical resistivity increases monotonically with the increase of $AgInSe_2$ content.

A drastic decrease of total thermal conductivity is realized with an impressive room-temperature value of 1.6 $Wm^{-1}K^{-1}$, demonstrating the effectiveness of $AgInSe_2$ alloying in reducing the thermal conductivity of GeTe. The introduced various point defects help suppress the lattice thermal conductivity and enhance Seebeck coefficient, which lead to a low electronic thermal conductivity as well (Fig. S1). A detailed analysis of the lattice thermal conductivities is performed in the following parts. Although the reduction of the thermal conductivity is significant, the increased electrical resistivity makes the *ZT* value show an overall decreasing tendency at temperatures higher than 600 K. At temperatures below 600 K, the decreased thermal conductivity manifests itself with an enhanced *ZT* value, which motivates us to further improve it at the low-temperature range by tuning the Seebeck coefficients.

3.2 Enhancing near room-temperature *ZT* by Bi doping

To tune the Seebeck coefficient, Bi doping is selected, as it has proved itself effective in reducing the hole concentrations and lattice thermal conductivity [40, 41]. Since the 8%$AgInSe_2$-alloyed GeTe sample (AIS8) has the highest room temperature *ZT* without any observable In-Te based secondary phases, the AIS8 sample was chosen as the control sample (0% Bi) for the Bi doping series.

A series of Bi-doped AIS8 samples were prepared, which can be indexed to α-GeTe phase with traces of Ge secondary phase (Fig. 3a). After the introduction of the larger Bi^{3+} (ionic radius: 103 pm), the diffraction peaks shift slightly to lower 2θ angles for GeTe phase [37]. The two peaks of the AIS8 sample at 2θ = 43° gradually merge together with increasing Bi content, which implies the ability of Bi to enhance the structural symmetry of rhombohedral GeTe [22, 23]. The elemental mapping again confirms the existence of Ge secondary phase (Fig. 3b and Fig. 3e), where other elements were homogenously distributed, indicating the successful doping of Bi.

After Bi doping, both the Seebeck coefficient and electrical resistivity (Fig. 4a and Fig. 4b) increase gradually with a maximum Seebeck coefficient of over 220 μV/K at room temperature, which indicates the effectiveness of Bi in reducing hole concentration. Furthermore, with the temperature increasing, Seebeck coefficient and electrical resistivity first increase and then decrease. This phenomenon implies the occurrence of bipolar conduction, which is discussed in greater detail in the **Supporting Information**. Also, the temperature for the Seebeck coefficient to reach the peak value gradually decreases when the doping content of Bi increases. This is most likely due to the reduced majority charge carrier concentration (holes in this case) upon Bi doping.

In order to further investigate the underlying mechanisms for the electrical transport properties, room temperature Seebeck coefficient and electrical resistivity of the samples were analyzed using the Jonker plot with the assumption of acoustic phonon scattering mechanism [42, 43] (Fig. 4c). It can be seen that $AgInSe_2$ alloying gradually degrades the electronic transport coefficients (σ_{E0}) from 109000 S/m to 38000 S/m. Such a dramatic decrease can be related to the large content of Indium introduced as In will significantly decrease the carrier mobility [36]. Whereas the Seebeck coefficient and electrical conductivity of Bi doped samples can be fitted with the same σ_{E0} curve. From the undeteriorated σ_{E0}, it can be concluded that Bi doping only causes minimal degradation to the intrinsic electronic transport properties of the AIS8 sample. The effectiveness of Bi doping in modulating the electrical properties can also be well-reflected in the plot of room-temperature thermoelectric power factor (PF = S^2/ρ) against Seebeck coefficient (Fig. 4d). Bi doping enables the attainment of the optimum range of Seebeck coefficients (140 – 230 μV/K), which are required to reach the theoretical maximum room-temperature PF. Finally, a high PF of ~ 11 $\mu Wcm^{-1}K^{-2}$ can be obtained at 300 K for a wide range of Bi doping contents (from y = 4 to 8 %).

Besides optimizing the room temperature PF, Bi doping also helps to greatly decrease the total thermal conductivity from ~1.9 $Wm^{-1}K^{-1}$ to ~0.7 $Wm^{-1}K^{-1}$ at 300 K (Fig. 5a). This decrease is attributed to the suppression of both the electronic thermal conductivity (Fig. S2) and the lattice

thermal conductivity (Fig. 5b). The room-temperature lattice thermal conductivity can be reduced to ~0.6 $Wm^{-1}K^{-1}$ after 8% Bi is introduced. While the rapid increase of thermal conductivity after 500 K is also caused by the bipolar effects, coinciding with the decrease of Seebeck coefficient and electrical resistivity mentioned above.

In order to understand the reduction of lattice thermal conductivity, the Callaway and Klemens' model is applied with the formula [45, 46]:

$$\kappa_{L,\,alloy}/\kappa_{L,\,Pure} = arc\tan(\mu)/\mu$$

Where μ is determined by:

$$\mu^2 = (\pi\theta_D\Omega/2\hbar v^2)\,\kappa_{L,\,Pure}\Gamma$$

θ_D denotes Debye temperature, Ω is the average volume per atom and v represents the average sound velocity. The calculation of the scattering parameter Γ can be divided into the mass term (Γ_M) and strain term (Γ_S), which can be determined by the following formula [45, 47]:

$$\Gamma_M = \frac{1}{2}\sum_{i=1}^{n}\left(\frac{\langle M_{Ge}\rangle}{\langle M^*\rangle}\right)^2 f_i(1-f_i)\left(\frac{\Delta M}{\langle M_{Ge}\rangle}\right)^2$$

$$\Gamma_S = \frac{1}{2}\sum_{i=1}^{n}\left(\frac{\langle M_{Ge}\rangle}{\langle M^*\rangle}\right)^2 f_i(1-f_i)\varepsilon\left(\frac{\Delta R}{\langle R_{Ge}\rangle}\right)^2$$

Where $\langle M_{Ge}\rangle$ and $\langle R_{Ge}\rangle$ represent the average mass and radius of the Ge sublattice, $\langle M^*\rangle$ is the average mass of the total sublattice, f_i is the concentration of i^{th} atom, ε is a parameter related to the elastic properties and is simulated, ΔM and ΔR denote the difference of mass and radius between the i^{th} atom and the host atom, respectively. Detailed values used in the simulation are summarized in the **Supporting Information**.

The room-temperature lattice thermal conductivity fits nicely in this point defect model (Fig. 5c). Thus, it can be concluded that the decrease of lattice thermal conductivity arises from the scattering of phonons by the abundant point defects. Although the reduction of κ_L is abrupt with a lower amount of $AgInSe_2$, the simulated curve indicates the degree of κ_L reduction becomes much less after many point defects are introduced. This means other phonon scattering sources like dislocations or planar defects are required to further reduce κ_L. A comparison of κ_L values at 300 K is also performed (Fig. 5d), where the low κ_L achieved in this work is less than or comparable with some reported data [22, 25, 29, 35, 44].

Due to the optimized PF and low κ_L achieved by Bi doping, the *ZT* value is enhanced to 0.46 at room temperature, as well as a high *ZT* value of 1.1 at 523 K. This enhancement is also well understood with a quality factor of 0.14 (Fig. 6b). The doping of Bi gradually enhances the Seebeck coefficient to the optimized range, while the deviation between the simulation and the experimental value is due to the variances of κ_L. It can also be noticed that using a minimum value of lattice thermal conductivity (κ_{Lmin}) based on the Debye-Cahill model [48], the *ZT* value can be further enhanced to ~0.6 at 300 K.

4 Conclusion

In this work, the near-room-temperature thermoelectric properties of GeTe was especially focused on. The alloying $AgInSe_2$ successfully decreased the lattice thermal conductivity from over 1.5 $Wm^{-1}K^{-1}$ in pristine GeTe to ~0.8 $Wm^{-1}K^{-1}$ in the 8% $AgInSe_2$-alloyed GeTe at 300 K. Moreover, it also leads to a higher Seebeck coefficient and electrical resistivity at 300 K, facilitating the decrease of electronic thermal conductivity. It was revealed that further doping with Bi optimizes the Seebeck coefficient without significantly damaging the intrinsic electrical transport properties of the matrix. Meanwhile, Bi doping also helps to lower the lattice thermal conductivity to 0.6 $Wm^{-1}K^{-1}$ at 300 K. The decrease of lattice thermal conductivity can be well explained by the scattering of phonons due to the various point defects introduced. Due to the synergetic effects of Bi in modulating the electrical and thermal transport properties, a largely enhanced *ZT* value of 0.46 at 300 K was achieved together with a high *ZT* value of 1.1 at 523 K.

Acknowledgments This work is financially supported by the Singapore MOE AcRF Tier 2 under Grant No.2018-T2-1-010, Singapore A*STAR project (A19D9a0096 and SC25/21-102419), Singapore MOE Tier 1 RG128/21. Q. Zhu and A. Suwardi acknowledge Agency for Science, Technology and Research (A*STAR), Singapore Career Development Fund (CDF) C210112022, Sustainable Hybrid Lighting System for Controlled Environment Agriculture programme: A19D9a0096. Z. Li thanks the support from S&T Program of Hebei (206Z4403G). The authors would also like to acknowledge the Facility for Analysis, Characterization, Testing and Simulation, Nanyang Technological University, Singapore, for use of their electron microscopy/X-ray facilities.

Conflicts of interest/Competing interests

The authors declare that they have no conflict of interest.

References

[1] Bell LE. Cooling, heating, generating power, and recovering waste heat with thermoelectric systems. Science. 2008;321(5895):1457-1461.
[2] Shi X-L, Zou J and Chen Z-G. Advanced Thermoelectric Design: From Materials and Structures to Devices. Chem Rev. 2020;120(15):7399-7515.
[3] Yan Q and Kanatzidis MG. High-performance thermoelectrics and challenges for practical devices. Nat Mater. 2021;1-11.
[4] Snyder GJ and Toberer ES. Complex thermoelectric materials. Nat Mater. 2008;7(2):101-110.
[5] Li J-F, Liu W-S, Zhao L-D and Zhou M. High-performance nanostructured thermoelectric materials. NPG Asia Mater. 2010;2(4):152-158.
[6] Zheng Y, Slade TJ, Hu L, Tan XY, Luo Y, Luo Z-Z, Xu J, Yan Q and Kanatzidis MG. Defect engineering in thermoelectric materials: what have we learned?. Chem Soc Rev. 2021;50(16):9022-9054.
[7] Zevalkink A, Smiadak DM, Blackburn JL, Ferguson AJ, Chabinyc ML, Delaire O, Wang J, Kovnir K, Martin J, Schelhas LT, Sparks TD, Kang SD, Dylla MT, Snyder GJ, Ortiz BR and Toberer ES. A practical field guide to thermoelectrics: Fundamentals, synthesis, and characterization. Appl Phys Rev. 2018;5(2):021303.

[8] Jia N, Cao J, Tan XY, Dong J, Liu H, Tan CKI, Xu J, Yan Q, Loh XJ and Suwardi A. Thermoelectric materials and transport physics. Mater Today Phys, 2021;21:100519.
[9] He J and Tritt TM. Advances in thermoelectric materials research: Looking back and moving forward. Science. 2017;357(6358):eaak9997.
[10] Zhao L-D, Tan G, Hao S, He J, Pei Y, Chi H, Wang H, Gong S, Xu H, Dravid VP, Uher C, Snyder GJ, Wolverton C and Kanatzidis MG. Ultrahigh power factor and thermoelectric performance in hole-doped single-crystal SnSe. Science. 2016;351(6269):141-144.
[11] Qin B, Wang D, Liu X, Qin Y, Dong J, Luo J, Li J-W, Liu W, Tan G, Tang X, Li J-F, He J and Zhao L-D. Power generation and thermoelectric cooling enabled by momentum and energy multiband alignments. Science. 2021;373(6554):556-561.
[12] Luo Y, Cai S, Hao S, Pielnhofer F, Hadar I, Luo Z-Z, Xu J, Wolverton C, Dravid VP, Pfitzner A, Yan Q and Kanatzidis MG. High-Performance Thermoelectrics from Cellular Nanostructured $Sb_2Si_2Te_6$. Joule, 2020;4(1):159-175.
[13] Zhao K, Liu K, Yue Z, Wang Y, Song Q, Li J, Guan M, Xu Q, Qiu P, Zhu H, Chen L and Shi X. Are Cu_2Te-Based Compounds Excellent Thermoelectric Materials?. Adv Mater. 2019;31(49):1903480.
[14] Liu H, Shi X, Xu F, Zhang L, Zhang W, Chen L, Li Q, Uher C, Day T and Snyder GJ. Copper ion liquid-like thermoelectrics. Nat Mater. 2012;11(5):422-425.
[15] Tamaki H, Sato HK and Kanno T. Isotropic Conduction Network and Defect Chemistry in $Mg_{3+\delta}Sb_2$-Based Layered Zintl Compounds with High Thermoelectric Performance. Adv Mater. 2016;28(46):10182-10187.
[16] Mao J, Zhu H, Ding Z, Liu Z, Gamage GA, Chen G and Ren Z. High thermoelectric cooling performance of n-type Mg_3Bi_2-based materials. Science. 2019;365(6452):495-498.
[17] Fu C, Bai S, Liu Y, Tang Y, Chen L, Zhao X and Zhu T. Realizing high figure of merit in heavy-band p-type half-Heusler thermoelectric materials. Nat Commun. 2015;6:1-7.
[18] Zeier WG, Schmitt J, Hautier G, Aydemir U, Gibbs ZM, Felser C and Snyder GJ. Engineering half-Heusler thermoelectric materials using Zintl chemistry, Nat Rev Mater. 2016;1(6):1-10.
[19] Hong M, Zou J and Chen Z-G. Thermoelectric GeTe with Diverse Degrees of Freedom Having Secured Superhigh Performance. Adv Mater. 2019;31(14):1807071.
[20] Zhang X, Bu Z, Lin S, Chen Z, Li W and Pei Y. GeTe Thermoelectrics. Joule. 2020;4(5):986-1003.
[21] Li J, Zhang X, Wang X, Bu Z, Zheng L, Zhou B, Xiong F, Chen Y and Pei Y. High-Performance GeTe Thermoelectrics in Both Rhombohedral and Cubic Phases. J Am Chem Soc. 2018;140(47):16190-16197.
[22] Li J, Zhang X, Chen Z, Lin S, Li W, Shen J, Witting IT, Faghaninia A, Chen Y, Jain A, Chen L, Snyder GJ and Pei Y. Low-Symmetry Rhombohedral GeTe Thermoelectrics. Joule. 2018;2(5):976-987.
[23] Dong J, Sun F-H, Tang H, Pei J, Zhuang H-L, Hu H-H, Zhang B-P, Pan Y and Li J-F. Medium-temperature thermoelectric GeTe: vacancy suppression and band structure engineering leading to high performance. Energy Environ Sci. 2019;12(4):1396-1403.
[24] Bu Z, Li W, Li J, Zhang X, Mao J, Chen Y and Pei Y. Dilute Cu_2Te-alloying enables extraordinary performance of r-GeTe thermoelectrics. Mater Today Phys. 2019;9:100096.
[25] Hong M, Wang Y, Liu WD, Matsumura S, Wang H, Zou J and Chen Z-G. Arrays of Planar Vacancies in Superior Thermoelectric $Ge_{1-x-y}Cd_xBi_yTe$ with Band Convergence. Adv Energy Mater. 2018;8(30):1801837.
[26] Wu D, Xie L, Xu X and He J. High Thermoelectric Performance Achieved in GeTe–Bi_2Te_3 Pseudo-Binary via Van der Waals Gap-Induced Hierarchical Ferroelectric Domain Structure. Adv Func Mater, 2019;29(18):1806613.
[27] Tsai Y-F, Wei P-C, Chang L, Wang K-K, Yang C-C, Lai Y-C, Hsing C-R, Wei C-M, He J, Snyder GJ and Wu H-J. Compositional Fluctuations Locked by Athermal Transformation Yielding High Thermoelectric Performance in GeTe. Adv Mater. 2020;33(1):2005612.
[28] Bai G, Yu Y, Wu X, Li J, Xie Y, Hu L, Liu F, Wuttig M, Cojocaru-Mirédin O and Zhang C. Boron Strengthened GeTe-Based Alloys for Robust Thermoelectric Devices with High Output Power Density. Adv Energy Mater. 2021;11(37):2021.
[29] Zhi S, Li J, Hu L, Li J, Li N, Wu H, Liu F, Zhang C, Ao W, Xie H, Zhao X, Pennycook SJ and Zhu T. Medium Entropy-Enabled High Performance Cubic GeTe Thermoelectrics. Adv Sci. 2021;8(12):2100220.
[30] Dong J, Pei J, Zhuang H-L, Hu H, Cai B and Li J-F. High-performance electron-doped $GeMnTe_2$: hierarchical structure and low thermal conductivity. J Mater Chem A. 2019;7(48)：27361-27366.
[31] Suwardi A, Cao J, Hu L, Wei F, Wu J, Zhao Y, Lim SH, Yang L, Tan XY, Chien SW, Yin Y, Zhou W-X, Mun Nancy WL, Wang X, Lim SH, Ni X, Li D, Yan Q, Zheng Y, Zhang G and Xu J. Tailoring the phase transition temperature to achieve high-performance cubic GeTe-based thermoelectrics. J. Mater Chem A. 2020;8(36):18880-18890.
[32] Cao J, Tan XY, Jia N, Lan D, Solco SFD, Chen K, Chien SW, Liu H, Tan CKI, Zhu Q, Xu J, Yan Q and Suwardi A. Improved zT in Nb_5Ge_3–GeTe thermoelectric nanocomposite. Nanoscale. 2022;14(2):410-418.
[33] Xing T, Song Q, Qiu P, Zhang Q, Gu M, Xia X, Liao J, Shi X and Chen L. High efficiency GeTe-based materials and modules for thermoelectric power generation. Energy Environ Sci. 2021;14(2):995-1003.
[34] Bu Z, Chen Z, Zhang X, Lin S, Mao J, Li W, Chen Y and Pei Y. Near-room-temperature rhombohedral $Ge_{1-x}Pb_xTe$ thermoelectrics, Mater Today Phys. 2020;15:100260.
[35] Zhang X, Bu Z, Shi X, Chen Z, Lin S, Shan B, Wood M, Snyder AH, Chen L, Snyder GJ and Pei Y. Electronic quality factor for thermoelectrics. Sci Adv. 2020;6(46):eabc0726.
[36] Wu L, Li X, Wang S, Zhang T, Yang J, Zhang W, Chen L and Yang J, Resonant level-induced high thermoelectric response in indium-doped GeTe. NPG Asia Mater. 2017;9(1):e343.
[37] Shannon RD. Revised effective ionic-radii and systematic studies of interatomic distances in halides and chalcogenides. Acta Crystallogr Sect A. 1976;32(5):751-767.
[38] Suwardi A, Cao J, Zhao Y, Wu J, Chien SW, Tan XY, Hu L, Wang X, Wang W, Li D, Yin Y, Zhou WX, Repaka DVM, Chen J, Zheng Y, Yan Q, Zhang G and Xu J. Achieving high thermoelectric quality factor toward high figure of merit in GeTe. Mater. Today Phys. 2020;14：100239.
[39] Liu ZH, Sato N, Guo QS, Gao WH and Mori T. Shaping the role of germanium vacancies in germanium telluride: metastable cubic structure stabilization, band structure modification, and stable N-type conduction. NPG Asia Mater. 2020;12(1):1-11.
[40] Perumal S, Samanta M, Ghosh T, Shenoy US, Bohra AK, Bhattacharya S, Singh A, Waghmare UV and Biswas K. Realization of High Thermoelectric Figure of Merit in GeTe by Complementary Co-doping of Bi and In. Joule. 2019;3(10):2565-2580.
[41] Li J, Chen Z, Zhang X, Sun Y, Yang J and Pei Y. Electronic origin of the high thermoelectric performance of GeTe among the p-type group IV monotellurides. NPG Asia Mater. 2017;9(3):e353.
[42] Hu L, Luo Y, Fang Y-W, Qin F, Cao X, Xie H, Liu J, Dong J, Sanson A, Giarola M, Tan X, Zheng Y, Suwardi A, Huang Y,

Hippalgaonkar K, He J, Zhang W, Xu J, Yan Q and Kanatzidis MG. High Thermoelectric Performance through Crystal Symmetry Enhancement in Triply Doped Diamondoid Compound Cu_2SnSe_3. Adv Energy Mater. 2021;11(42):2100661.
[43] Kuo JJ, Kang SD, Imasato K, Tamaki H, Ohno S, Kanno T and Snyder GJ. Grain boundary dominated charge transport in Mg_3Sb_2-based compounds. Energy Environ Sci. 2018;11(2):429-434.
[44] Liu Z, Sun J, Mao J, Zhu H, Ren W, Zhou J, Wang Z, Singh DJ, Sui J, Chu CW and Ren Z. Phase-transition temperature suppression to achieve cubic GeTe and high thermoelectric performance by Bi and Mn codoping. Proc Natl Acad Sci USA. 2018;115(21):5332-5337.
[45] Wang H, LaLonde AD, Pei Y and Snyder GJ. The Criteria for Beneficial Disorder in Thermoelectric Solid Solutions. Adv Func Mater. 2013;23(12):1586-1596.
[46] Callaway J and von Baeyer HC. Effect of Point Imperfections on Lattice Thermal Conductivity. Phys Rev. 1960;120(4):1149.
[47] Dong J, Sun F-H, Tang H, Hayashi K, Li H, Shang P-P, Miyazaki Y and Li J-F. Reducing Lattice Thermal Conductivity of MnTe by Se Alloying toward High Thermoelectric Performance. ACS Appl Mater Interface. 2019;11(31):28221-28227.
[48] Cahill DG, Watson SK and Pohl RO. Lower limit to the thermal conductivity of disordered crystals. Physl Rev B. 1992;46(10):6131.

摘要 (Chinese Abstract)
GeTe 在 600K 以上具有很高的 *ZT* 值，是优异的中温区热电材料。由于 GeTe 的本征载流子浓度过高，因此其近室温的热电性能并没有得到过多的关注。在本工作中，我们通过 $AgInSe_2$ 合金化及 Bi 的掺杂，成功地将 GeTe 的室温 Seebeck 系数从 30 μV/K 提升到了 220 μV/K。我们发现，Bi 能够在优化 Seebeck 系数的同时，不损坏基体的本征电输运性能。一系列的 Bi 掺杂样品均具有高达 11 $\mu Wcm^{-1}K^{-2}$ 的功率因子。同时引入的大量点缺陷可以引起质量和应力波动，从而将室温的晶格热导率降低至 0.6 $Wm^{-1}K^{-1}$。得益于 Bi 掺杂在 $AgInSe_2$ 合金化 GeTe 中的协同效应，我们获得了 0.46 的室温 *ZT* 值，同时在 523K 获得了高达 1.1 的 *ZT* 峰值。

Figures

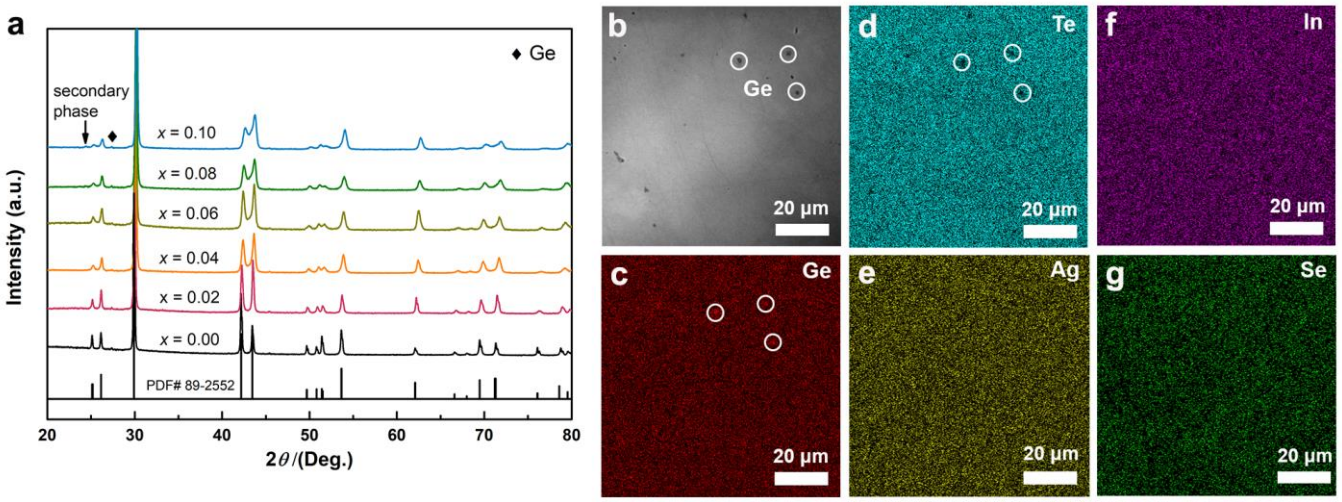

Fig.1 **a** XRD patterns of (1-*x*)GeTe-*x*AgInSe$_2$, **b** SEM image on polished surface of AIS8 sample, elemental distribution of **c** Ge, **d** Te, **e** Ag, **f** In and **g** Se.

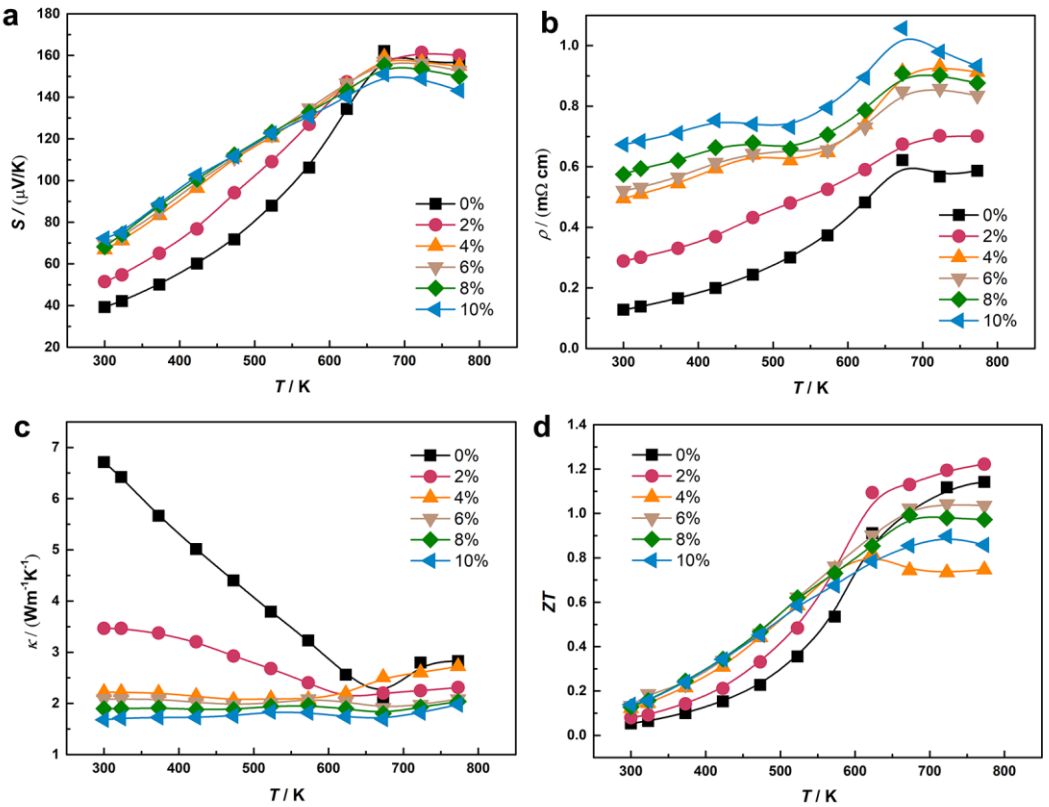

Fig. 2 **a** Seebeck coefficient, **b** electrical resistivity, **c** total thermal conductivity and **d** ZT value of (1-*x*)GeTe-*x*AgInSe$_2$ as a function of temperature.

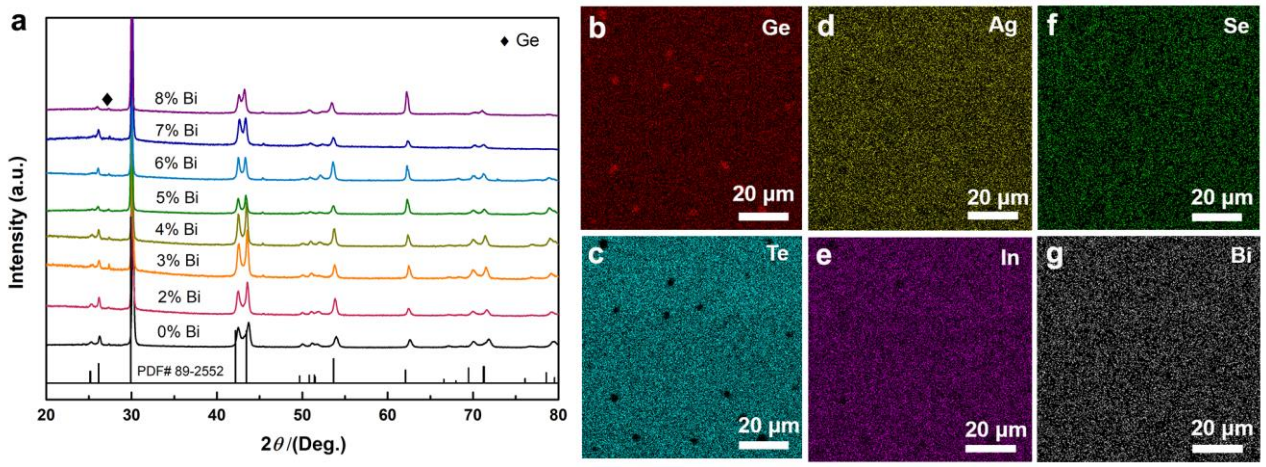

Fig.3 **a** XRD patterns of Bi-doped AIS8 samples, elemental distribution of **b** Ge, **c** Te, **d** Ag, **e** In, **f** Se and **g** Bi collected on the polished surface of AIS8-Bi7 sample.

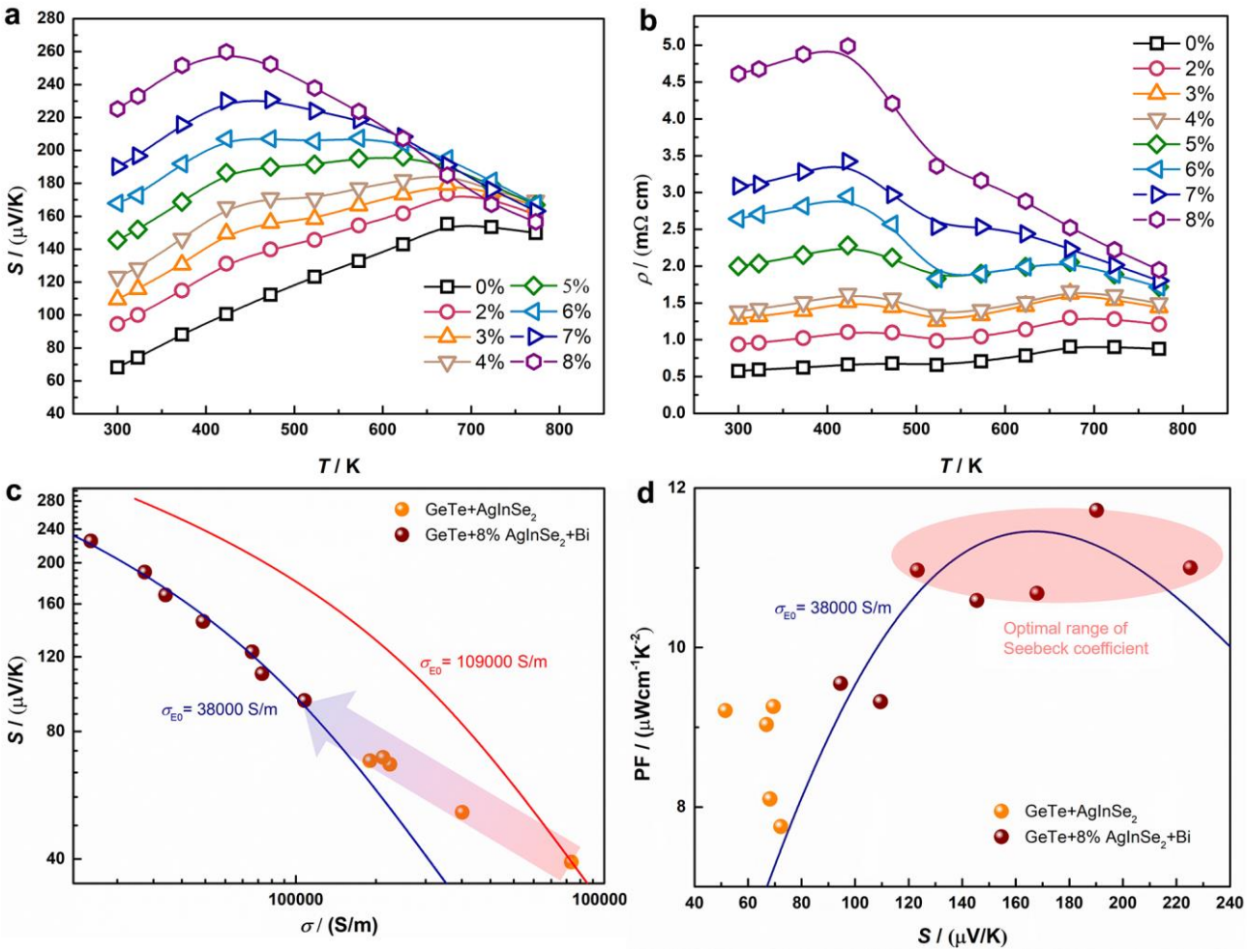

Fig.4 Temperature dependent **a** Seebeck coefficients and **b** electrical resistivities of AIS8-Biy samples, **c** Jonker plot of electrical conductivity as a function of Seebeck coefficient with the assumption of an acoustic phonon scattering dominated mechanism. **d** Seebeck coefficient dependence of power factor (PF) as well as the simulated curve with σ_{E0}=38000 S/m.

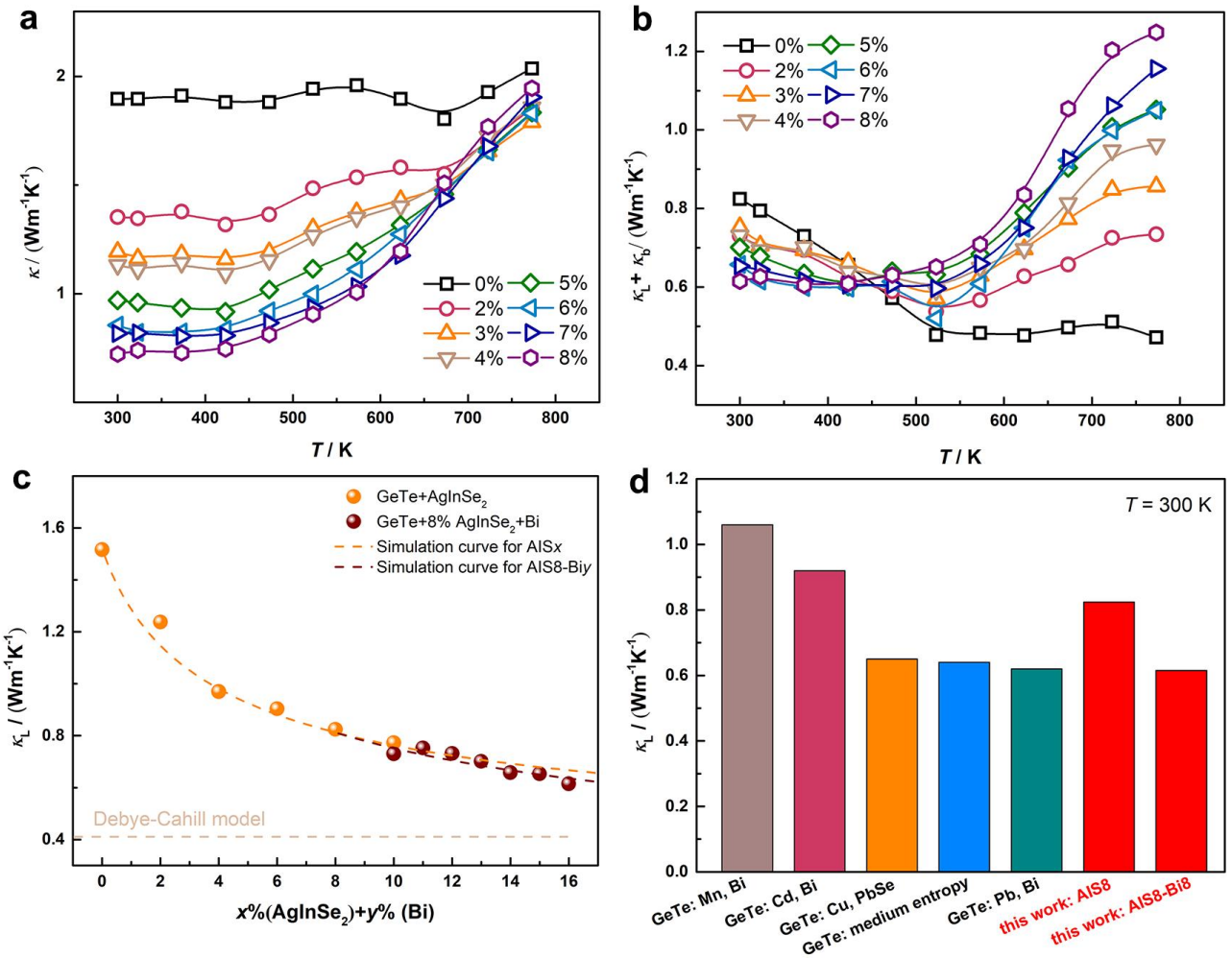

Fig.5 Temperature dependent **a** total thermal conductivity and **b** lattice and bipolar thermal conductivity of AIS8-Bi*y* samples, **c** composition dependence of lattice thermal conductivity at 300 K. The dashed curves were simulated using a point defect model. **d** Comparison of lattice thermal conductivity at 300 K between this work and literature data [22, 25, 29, 35, 44].

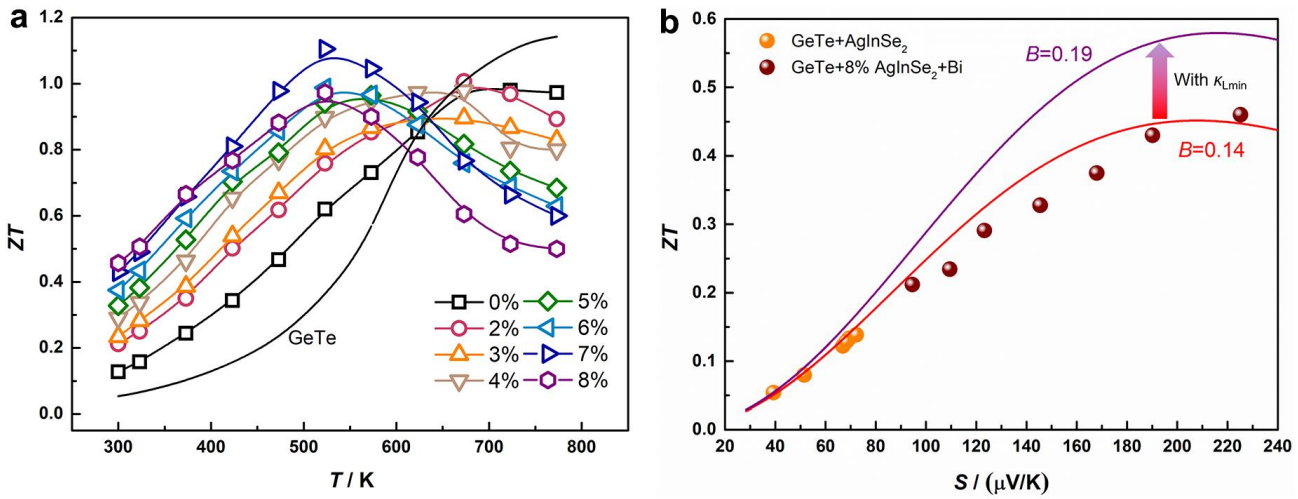

Fig.6 **a** Temperature dependent *ZT*, **b** relationship between *ZT* and Seebeck coefficient, the curves are simulated using quality factors of 0.14 and 0.19.

TOC (Table of Content)